Pore Evolution in Refractory Gold Ore Formed by Oxidation Roasting and the Effect on the Cyanide Leaching Process

Hui Li, Zhihang Li,* Jianping Jin,* Yuexin Han, and Yanjun Li

Read Online

ACCESS | Metrics & More | Article Recommendations | Supporting Information

ABSTRACT: Refractory gold ore is usually affected by the associated carbonaceous matter through the preg-robbing effect, which is eliminated by oxidation roasting, followed by leaching, to achieve a satisfactory gold leaching efficiency. Roasting−leaching experiments, pore structure measurements, scanning electron microscopy (SEM), and X-ray diffraction are used to explore the structural evolution of pores on the surface and its effect on the leaching performance. Pores with optimal sizes were obtained by roasting at 650 °C for 2.0 h with a ventilation of 0.6 m³/h; approximately 92.55% gold could be recovered under these conditions. A porous structure observed by SEM became more compact as the temperature further increased to 850 °C. The formation of $CaSiO_3$ and $CaSO_4$ in pores led to pore shrinkage. The mechanism of oxidation roasting, followed by cyanide leaching, was schematically analyzed and revealed the effects of pore structural evolution and phase transformation on the leaching efficiency.
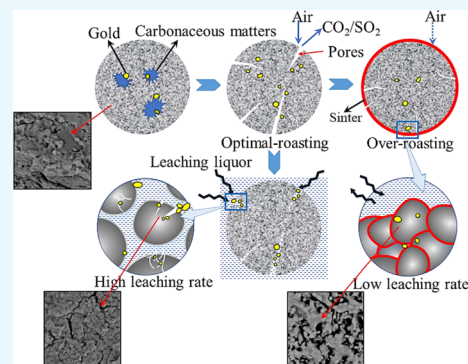
INTRODUCTION

Gold is a strategic mineral resource with financial attributes. China's gold consumption has remained the world's largest for consecutive years, and its production has ranked first in the world for 10 years.[1,2] However, the amount of easily exploited high-grade gold ores has rapidly decreased. Thus, the gold ore associated with carbonaceous matter (organic carbon and graphitic carbon), sulfur, and arsenic has become the major resource in gold production and faces many problems.[3−6]

Fine-grained carbonaceous gold ore is always enclosed by nonferrous minerals and is associated with carbonaceous matter and other gangue minerals.[7−9] Previous studies have validated the preg-robbing phenomenon, in which large amounts of gold are adsorbed on carbonaceous substances during the leaching process, such as the preg-robbing phenomena in the cyanidation of sulfide gold ores and the preg-robbing of gold from cyanide and noncyanide complexes.[10−13] Several studies have been conducted to reduce the adverse effects of inclusion and adsorption. Various utilization methods have realized engineering applications, such as oxidation roasting, bio-oxidation, flotation, pressure oxidation, and chemical oxidation.[14−19] Bio-oxidation is an eco-friendly method that has many advantages. A two-stage microbial process is used to destroy both sulfides and carbonaceous matter. In the first stage, bacteria were used to oxidize sulfides, and in the second stage, carbonaceous matter is destroyed using the bacterium. After degradation of carbonaceous matter in the second stage, cyanidation results in 94.7% gold extraction, which has increased by 13.6% compared to the extraction result in the first stage. However, the reaction speed is very slow, which takes over 20 days or even a longer time to

finish the bacterial pretreatment.[20,21] Moreover, pressure oxidation needs high pressure and high temperature to accelerate the oxidation process through the elimination of thin-film sulfide and arsenide coatings from gold surfaces, leading to easy cyanide access to gold. However, the strict requirements for equipment and the high operating cost are still big problems.[22−25] Chemical oxidation can provide good results, and chlorination roasting is a promising method that can obtain gold recovery of 92% at 800 °C with a roasting time of 4 h. Nevertheless, the high roasting temperature and the long roasting time have restricted its wide commercial application.[26,27] Flotation has been used to separate gold from raw ore, but the recovery of gold concentrates is unsatisfactory unless followed by other treatment methods. Flotation−preoxidation−cyanidation methods are used to improve recovery of refractory gold, but the gold recovery is limited to 72.2% after only treatment by the flotation process.[28] The development of oxidation roasting technologies has improved the market prospects of dealing with gold ore and other refractory ores despite the problems of over-roasting and under-roasting.[29,30] Oxidation roasting, followed by leaching, is considered as the optimum method to treat carbonaceous gold ore. In the two-stage roasting process
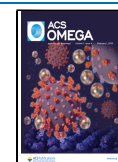
previously reported, the removal efficiency of arsenic and sulfur reached 96.98 and 97.19%, respectively. In this progress, gold could be effectively recovered from the refractory gold ore with a recovery of 98.06%.[31] However, most previous studies focused on the dynamics and thermodynamics of roasting, in which dynamic parameters were calculated and the potential reactions were discussed, but the effects of structural change after roasting were ignored. Therefore, increased attention should be paid to the microstructure of the surfaces and pores that formed on the roasted product, which have a direct impact on the leaching efficiency. Furthermore, several studies have shown that the porosity was improved by decomposing the carbonate compounds, while the channels in particles were cleared by evaporating the combined water.[32,33] The pore structure of diatomite was changed after second calcination at low temperature, while the number of micropores and mesopores increased significantly.[34] All the aforementioned studies confirm that various roasting conditions have a strong impact on pore structures. Therefore, systematic and theoretical research on the pore structure in the gold roasting−leaching process could promote the widespread application of oxidation roasting pretreatment in gold separation.

In this study, systematic roasting−leaching experiments on carbonaceous gold ore were carried out to explore the structural evolution of pores and provide evidence on the mechanism of pretreatment roasting in the leaching process. Pore size measurements, scanning electron microscopy (SEM), and X-ray diffraction (XRD) analysis were used to obtain insights into the changes in pore structure. This paper will provide theoretical and technical guidance on the efficient recovery of gold from carbonaceous fine-grained ores.

■ MATERIALS AND METHODS

Materials and Experimental Methods. The sample used in this study was obtained from a carbonaceous gold mine in Shaanxi province, China. Subsequently, 20 kg blocks were sorted out from 20 t of raw ore, and the sample was obtained after grinding and screening. The XRD result shows that the main mineral phases in the carbonaceous gold ore are quartz, dolomite, graphite, calcite, and pyrite. The result of chemical phase analysis of carbon indicates that the total carbon content is 6.39%, including 1.33% organic carbon and 1.50% graphitic carbon, which can adsorb solubilized gold cyanide as activated carbon.[35] The remaining 3.56% of carbon comes from carbonate minerals. The gold grade of raw ore is 5.46 g/t, which is determined by foamed plastic-enriched atomic absorption spectrophotometry. The results of the chemical composition analysis of gold minerals are listed in Table 1 and reveal that over 95% of minerals bearing gold are native gold.

Roasting tests were carried out in an HB-J-30 rotary resistance-heated furnace with a drum rotation speed of 4 rpm, as shown in Figure 1. First, 500 g samples were placed in the furnace for 2.0 h of roasting at a preset temperature and a ventilation of 0.8 m³/h to determine the change in pore structure. Then, the effects of ventilation capacity and roasting time were discussed. Finally, the roasted products were cooled to room temperature for weighing. The gold grade β of calcinate is calculated as follows

$$\beta = \frac{m_1}{m_0} \times \alpha \tag{1}$$

Table 1. Chemical Composition Analysis of Gold-Bearing Minerals

| points | composition and content/% | | |
	Au	Ag	total
1	95.53	4.47	100.00
2	95.23	4.77	100.00
3	100.00	0.00	100.00
4	88.69	11.31	100.00
5	100.00	0.00	100.00
6	100.00	0.00	100.00
average	96.58	3.43	100.00

where α is the grade of gold in raw ore, β is the grade of gold in calcinate, m_0 is the mass of the raw ore, and m_1 is the mass of the roasted product.

The oxidation roasting experiment, followed by leaching, is used to treat the samples. These were first ground in a Φ 160 mm × 240 mm wet rod mill to enable 80% of particles to pass through a 0.074 mm screen. Then, the slurry was added to the agitation leaching trough (model: XJTII, Changchun, China), followed by stirring for 5 min with a liquid-to-solid ratio of 2.5:1. Next, the pH was increased to 11 by adding CaO, and stirring was continued for 30 min. Gold leaching lasted 24.0 h with a concentration of 0.3% NaCN. The leaching residue was filtered and dried before measuring the gold grade. The leaching rate of gold (η) is calculated as follows[29,36]

$$\eta = \left(1 - \frac{\theta}{\beta}\right) \times 100\% \tag{2}$$

where η is the leaching rate of gold, β is the gold grade of calcinate, and θ is the gold grade of the leaching residue.

Analysis Methods. The amount of gold in solution was determined by inductively coupled plasma emission spectroscopy. The carbon content of solid samples was analyzed using a high-frequency infrared carbon−sulfur analytical instrument (HCS, HCS-800, Kaide Instruments Co.). The crystallographic composition of the samples was determined using a PW3040 XRD system (Panalytical B.V., Holland) using Cu Kα radiation (λ = 1.541 Å) at 40 kV and 35 mA in 2θ ranging from 5 to 70°. The original data of the samples were analyzed with the HighScore Plus software. SEM with energy-dispersive X-ray spectroscopy (EDS) analysis was conducted using a Quanta 650 scanning electron microscope (FEI, Hillsboro, USA) coupled with a double X-ray spectrometer (AMETEK, Inc., Berwyn, USA) for electron image acquisition and elemental analysis, respectively. Different magnifications (up to ×2000) were used for secondary electron images. Imaging studies were also conducted in specific microscopic areas of the samples to evaluate the distribution of elements throughout the sample.[37] N₂ adsorption/desorption isotherms were acquired at a liquid nitrogen temperature of −196 °C after pretreatment in vacuum for 2.0 h at 200 °C. The pore structure and specific surface area of the ore and calcinate were measured using a surface area and porosity analyzer (ASAP2020, Micromeritics, America). The surface area and porosity were determined by applying the Brunauer−Emmett−Teller (BET) equation and Barrett, Joyner, and Halenda method, respectively, to the desorption branch of isotherms based on capillary decondensation. Theoretically, the volume of the internal pores of calcinate was calculated through the
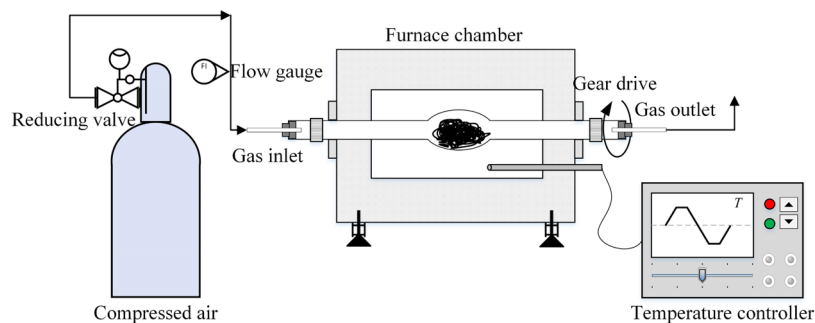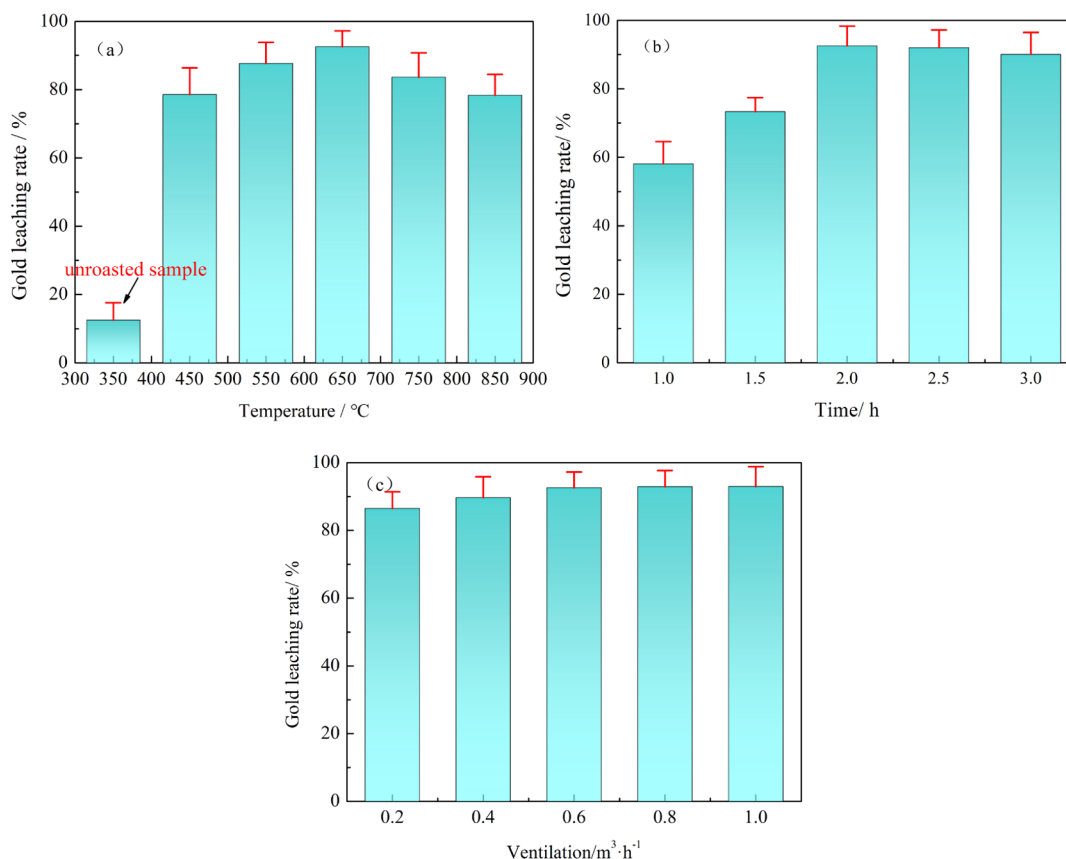
Figure 1. Roasting system used in experiments.

Figure 2. Effect of roasting temperature (a), time (b), and ventilation (c) on the gold leaching rate.

pressure.[38−40] The liquid mercury consumption volume is expressed as follows

$$D = -\frac{4\gamma \cos \vartheta}{p} \tag{3}$$

where D is the diameter of the inner hole of calcinate, γ is the surface tension of mercury, ϑ is the contact angle between liquid mercury and the hole in calcinate, and p is the applied mercury pressure.

■ RESULTS AND DISCUSSION

Effects of Oxidation Roasting on Leaching Results. To determine the effects of roasting on gold leaching, roasting−leaching experiments were carried out under various conditions. First, the ventilation was maintained at 0.8 m³/h, and the roasting time was 2.0 h. The results in Figure 2a show that the gold leaching rate of the sample without high-

temperature pretreatment remained at a low level of 12.50%. With the increase in temperature, the gold leaching rate increased to approximately 92.5% at 650 °C and then exhibited a downward trend beyond 650 °C. The results showed that oxidation roasting at 650 °C limited the preg-robbing effect. The effect of roasting time on the gold leaching rate at 650 °C with a ventilation capacity of 0.8 m³/h is shown in Figure 2b. When the roasting time increased from 1.0 to 2.0 h, the gold leaching rate increased from 58.09 to 92.5%. When the roasting time reached 3.0 h, the gold leaching rate showed a slight decrease. Therefore, a prolonged roasting time did not increase the gold leaching rate. Ventilation provides oxygen for the oxidation reaction of carbonaceous substances and pyrite, which also affect the experimental results as shown in Figure 2c. With the increase in ventilatory capacity, the gold leaching rate showed a slight increase. When the ventilation capacity exceeded 0.6 m³/h, no effect on the leaching rate was observed. The abovementioned results indicate that temper-
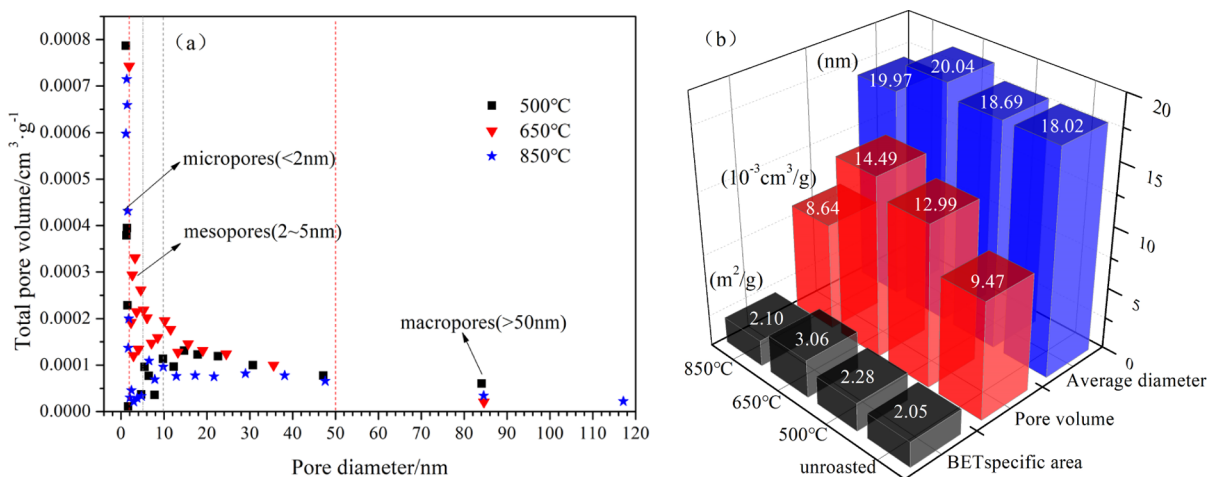
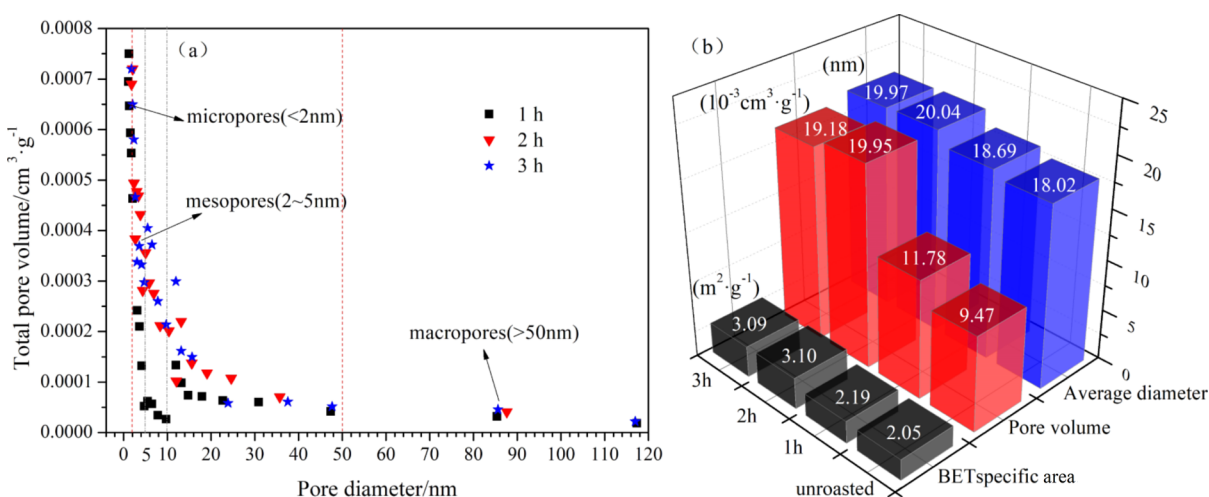**Figure 3.** Pore diameter distribution (a) and parameter (b) of calcinate at different temperatures.

Figure 4. Pore diameter distribution (a) and parameter (b) of calcinate after roasting for 1.0, 2.0, and 3.0 h.
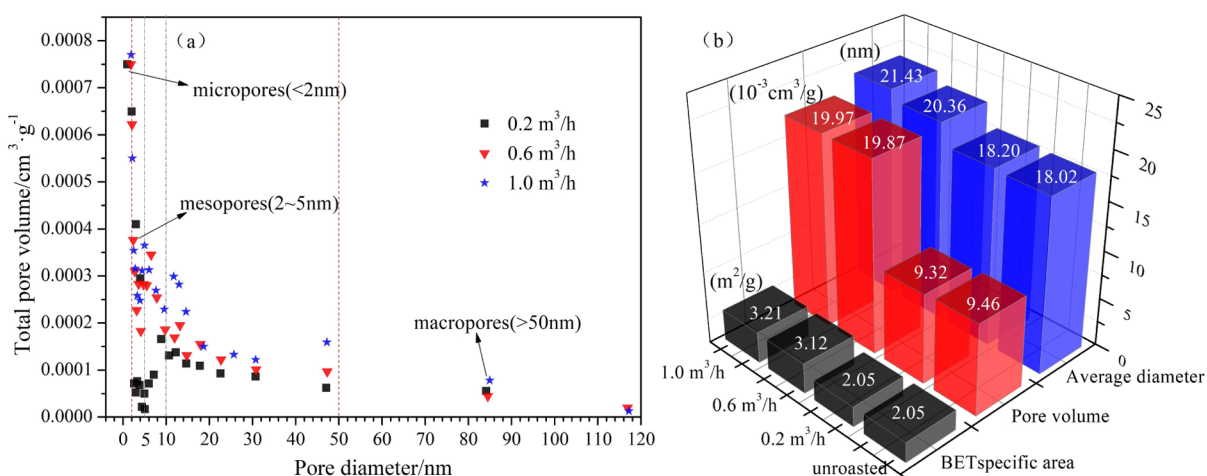

Figure 5. Pore diameter distribution (a) and parameters (b) of calcinate at 0.2, 0.6, and 1.0 m^3/h.

ature has the greatest influence on the leaching result, followed by the roasting time; the effect of ventilation capacity is negligible.

Effect of Roasting on Pore Size Distribution. Physicochemical reactions occur during the roasting process, such as the oxidation of carbonaceous substances and pyrite,

and the decomposition of carbonate minerals with the release of gas, which lead to changes in the surface structure. Pores emerge in the inner space between different particles after the reactions occurred, which may contribute to the progression of leaching reaction. The pore structure is closely related to the roasting temperature and roasting time, while the pore size
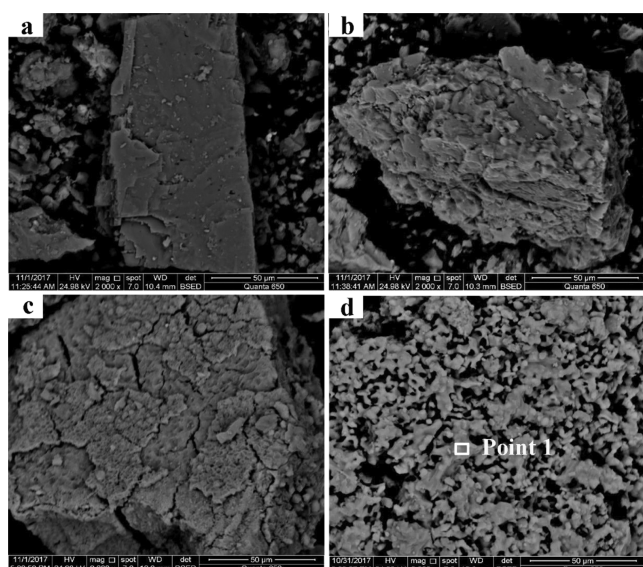
Figure 6. SEM images of raw ore and calcinate at different temperatures: (a) raw ore, (b) roasted at 500 °C, (c) roasted at 650 °C, and (d) roasted at 850 °C.
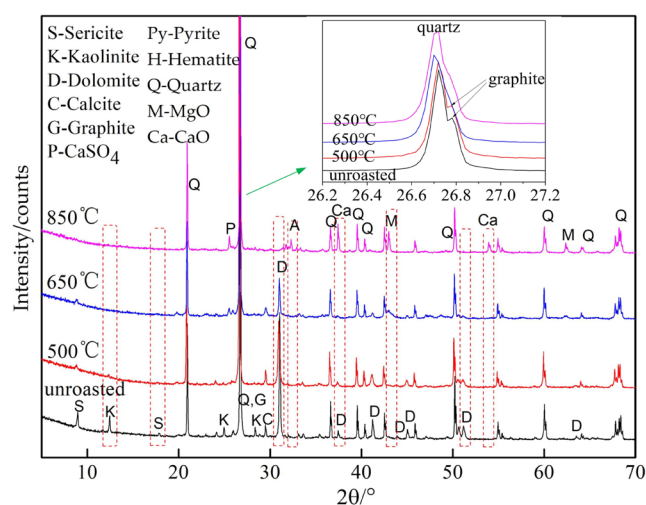

Figure 7. XRD image of unroasted and roasted products at 500, 650, and 850 °C.

distribution varied with roasting conditions. The rules of the International Union of Pure and Applied Chemistry classify pores into three types according to their diameters: micropore (<2 nm), macropore (>50 nm), and mesopore (2−50 nm).

The pore size distributions at different temperatures are shown in Figure 3a. At 500 °C, large numbers of micropores were detected. As the temperature increased to 650 °C, micropores decreased significantly and more mesopores appeared, especially those with diameters of 2−10 nm. At 850 °C, the total pore volume of mesopores sharply decreased, especially 2−5 nm mesopores, and more micropores appeared. The pore parameters of samples roasted at 500, 650, and 850 °C, such as specific surface area, pore volume, and average

diameter, are shown in Figure 3b. With the increase in temperature, all parameters mentioned above exhibited an upward trend that reached peak values at 650 °C. Better leaching results were also obtained at 650 °C as there were more mesopores, indicating that an increase in pore size could improve the gold leaching rate. However, the total pore volume showed a huge decrease from 14.48×10^{-3} to 8.63×10^{-3} cm^3/g when the temperature reached 850 °C. An excessively high temperature caused the decrease and closure of pores, which limited the diffusion of leachate and decreased the leaching results.

Pore size distributions at different roasting times are shown in Figure 4a. It reveals that most pores are 1−2 nm micropores after roasting for 1.0 h and the pore volume of 5−10 nm mesopores remained at a low level. After roasting for 2.0 h, micropores sharply decreased, while 2−10 nm mesopores increased significantly. After 3.0 h, the pore size did not exhibit any obvious change; hence, the leaching results did not show a remarkable change. Therefore, a sufficient roasting time is beneficial to the increase in pore size. The pore parameters of samples roasted for different times are shown in Figure 4b. The BET specific area increased with time, and the growth rate reached a peak as the time increased from 1.0 to 2.0 h. The same upward trend was observed for the pore volume and diameter, which proves that more pores were formed during this period, which benefits the diffusion of leaching liquor in the porous structure. Although slight decreases in pore volume and pore size were detected at 3.0 h, these had little influence on the leaching result.

Pore size distributions with different ventilation capacities are shown in Figure 5a. The change in pore size is closely related to the ventilation capacity. As the ventilation capacity increased from 0.2 to 0.6 m^3/h, the total pore volume reached 19.87×10^{-3} cm^3/g. Compared with the pores measured at over 0.6 m^3/h, more 1−2 nm micropores were detected at 0.2 m^3/h, which was attributed to the incomplete chemical reactions at a low oxygen concentration. With the increase in ventilation, a large amount of gas is released owing to the oxidation of pyrite and carbonaceous matter. As a result, 1−2 nm micropores could not be detected, and a majority of pores were mesopores with diameters of 5−20 nm. The pore parameters of the roasted product with different ventilations are shown in Figure 5b. A significant increase was observed in pore volume with the increase in ventilation from 0.2 to 0.6 m^3/h. This directly proves that increasing the oxygen concentration could significantly improve the pore size. However, excessive ventilation (>0.6 m^3/h) does not have a significant effect on the pore structure, and the pore volume only displayed a slight increase from 19.87×10^{-3} to 19.98×10^{-3} cm^3/g as the ventilation increased to 1.0 m^3/h.

Effect of Pore Structure on the Leaching Process. The leaching results indicate that the effect of temperature was the most significant. Previous studies have shown that roasting temperature dominates the process of chemical reactions and phase transformation in multiple minerals, leading to changes in the surface structure and components. Therefore, the effect

Table 2. EDS Analysis of Calcinate at 850 °C

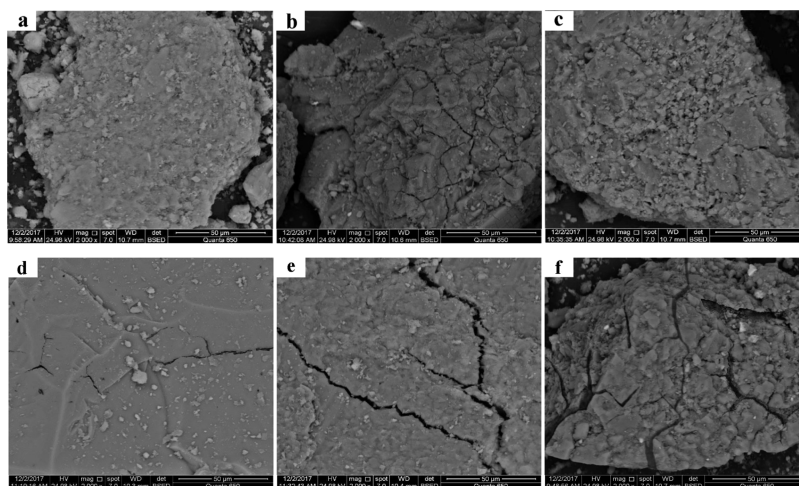| elements	O	Si	Ca	K	Mg	Fe	V	Ti	total
content/%	63.41	17.73	12.26	4.24	1.27	0.62	0.26	0.21	100

Figure 8. SEM images of calcinate roasted for different times: (a) roasted for 1.0 h, (b) roasted for 2.0 h, and (c) roasted for 3.0 h; SEM images of calcinate at different ventilations: (d) roasted at 0.2 m³/h, (e) roasted at 0.6 m³/h, and (f) roasted at 1.0 m³/h.
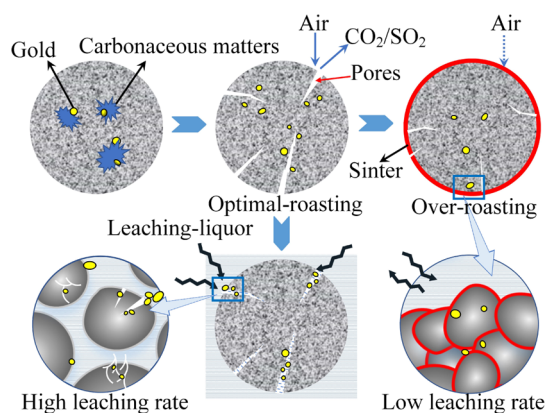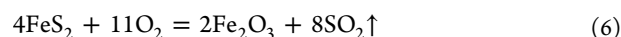

Figure 9. Schematic diagram of the oxidation roasting process.

of temperature on the structure was systematically studied, and the influence of time and ventilation was discussed.

SEM images of samples at different temperatures are shown in Figure 6 to provide insight into the surface structure. More pores were observed on the surface at 500 °C compared with raw ore. At 650 °C, more cracks appeared and expanded to form a loose and porous structure. The sample roasted at 850 °C showed a special structure in which spheroidal particles were generated and then connected with each other, as shown in Figure 6d. Although large channels were observed between the roasted particles, almost no pores or cracks were found inside this compact combination.

The XRD images of unroasted and roasted products in Figure 7 show the changes and reactions that occurred at 500, 650, and 850 °C. The curve of the unroasted sample showed that the raw ore mainly consisted of dolomite, calcite, kaolinite, and other carbon-bearing minerals such as graphite. At 500 °C, dolomite started to decompose, and the typical diffraction peaks weakened at 650 °C. These peaks were not observed at 850 °C, but peaks of CaO and MgO appeared, which are expressed as eq 4. Calcite decomposed at 650 °C, and peaks disappeared at 850 °C, as expressed in eq 5. Graphite and pyrite reacted with oxygen to generate pore structures because of the release of CO_2 and SO_2 as the temperature increased beyond 500 °C, as represented in eq 6. The partially enlarged view shows that the graphite peaks disappeared at above 650

°C, indicating that graphite was completely oxidized. At 850 °C, decomposition reactions were completed and new phases were formed, such as $CaSO_4$ and $CaSiO_3$, as shown in eqs 7 and 8, respectively. Because the gas could only escape from the pores, part of new phases would be located at these positions

$$CaMg(CO_3)_2 = CaO + MgO + 2CO_2\uparrow \qquad (4)$$

$$CaCO_3 = CaO + 2CO_2\uparrow \qquad (5)$$

$$4FeS_2 + 11O_2 = 2Fe_2O_3 + 8SO_2\uparrow \qquad (6)$$

$$CaO + SiO_2 = CaSiO_3 \qquad (7)$$

$$2CaO + 2SO_2 + O_2 = 2CaSO_4 \qquad (8)$$

Owing to the decomposition of carbon-bearing minerals, such as dolomite and calcite, and the oxidation of pyrite at 650 °C, a large amount of gas was released to form more mesopores. This facilitated the diffusion of leaching liquor in the roasted products. The zone marked in Figure 6d was analyzed by EDS, and the results are presented in Table 2. No C element was found in the marked position, indicating that the carbonaceous substance had completely oxidized or decomposed. Despite the elimination of the preg-robbing effect of carbonaceous matter, mesopores started to disappear and a compact structure was formed because of the filling of newly generated phases with a low melting point at high temperature. Consequently, the leaching efficiency decreased at temperatures exceeding 650 °C.

Samples roasted for different times at 650 °C are shown in Figure 8a−c. Few micropores were observed after roasting for 1.0 h. After 2.0 h, more pores were detected and cracks began to form on the surface. However, crack closure occurred after heating for 3.0 h. Therefore, a prolonged roasting time has a detrimental effect on leaching because of the closure of cracks and pores. Products roasted with different ventilations were scanned by SEM, as shown in Figure 8d−f. It was found that increasing ventilation promoted the formation of pores and cracks. A few small shadow cracks appeared on the surface as the ventilation reached 0.2 m³/h. Larger cracks were observed at 0.6 and 1.0 m³/h, but the microstructures did not show a fundamental difference. Therefore, the effect of increasing ventilation on leaching rate is inconspicuous when it over 0.6 m³/h.

The air roasting process of carbonaceous gold ore is illustrated schematically in Figure 9. During the under-roasting process, carbonaceous substances and carbonated minerals were closely associated and functioned with gold to form inclusions, leading to a low gold leaching rate. Under optimal conditions, carbonaceous matter was cleared; hence, the preg-robbing effect was eliminated. The release of CO_2 and SO_2 also contributed to the formation of a porous structure.[41,42] Therefore, a high gold leaching rate was obtained under these conditions, as shown in Figure 3. After over-roasting, newly formed substances filled the pores and cracks, and sinters were generated, resulting in a compact structure, which deteriorated the leaching environment significantly.

CONCLUSIONS

The oxidation roasting−leaching results revealed that the optimum roasting conditions were 650 °C with a ventilation of 0.6 m^3/h for 2.0 h, at which the gold leaching rate reached a peak value of 92.5%. Pores were significantly affected by the roasting temperature, followed by the roasting time and ventilation. More mesopores and macropores could improve the leaching rate, while an excessively high roasting temperature and a long roasting time restricted the growth of pores. Owing to the high temperature (>650 °C) and the long roasting time (>2.0 h), $CaSO_4$ and $CaSiO_3$ with low melting points were formed, leading to the closure of pores and poor leaching performance.

ASSOCIATED CONTENT

Supporting Information

The Supporting Information is available free of charge at https://pubs.acs.org/doi/10.1021/acsomega.1c06248.

> Results of the XRD spectrum and chemical phase analysis to show the mineral phase composition and chemical phase of carbon in raw ore, which contributes to the understanding of the preg-robbing effect caused by carbonaceous matters (PDF)

AUTHOR INFORMATION

Corresponding Authors

Zhihang Li − School of Earth Science and Resources, Chang'an University, Xi'an 710054, China; orcid.org/0000-0002-7575-761X; Email: neulizhihang@sina.com

Jianping Jin − School of Resources and Civil Engineering, Northeastern University, Shenyang 110004, China; Email: jin20030944@126.com

Authors

Hui Li − School of Resources and Civil Engineering, Northeastern University, Shenyang 110004, China

Yuexin Han − School of Resources and Civil Engineering and State Key Laboratory of Rolling and Automation, Northeastern University, Shenyang 110004, China; National-Local Joint Engineering Research Center of High-Efficient Exploitation Technology for Refractory Iron Ore Resources, Shenyang 110004, China

Yanjun Li − School of Resources and Civil Engineering, Northeastern University, Shenyang 110004, China; National-Local Joint Engineering Research Center of High-Efficient Exploitation Technology for Refractory Iron Ore Resources, Shenyang 110004, China

Complete contact information is available at:

Notes

The authors declare no competing financial interest.

ACKNOWLEDGMENTS

REFERENCES

(1) Liu, X.; Li, Q.; Zhang, Y.; Jiang, T.; Yang, Y.; Xu, B.; He, Y. Improving gold recovery from a refractory ore via Na 2 SO 4 assisted roasting and alkaline Na 2 S leaching. Hydrometallurgy 2019, 185, 133−141.

(2) Wang, H.; Feng, Y.; Li, H.; Kang, J. The separation of gold and vanadium in carbonaceous gold ore by one-step roasting method. Powder Technol. 2019, 355, 191−200.

(3) Luo, W.; Yang, H.; Qiu, X.; Li, H. Bacterial oxidation and cyanide leaching process for carbonaceous carlin-type gold deposit. J. Northeast Univ., Nat. Sci. 2014, 35, 1579−1582.

(4) Konadu, K. T.; Harrison, S. T. L.; Osseo-Asare, K.; Sasaki, K. Transformation of the carbonaceous matter in double refractory gold ore by crude lignin peroxidase released from the white-rot fungus. Int. Biodeterior. Biodegrad. 2019, 143, 104735.

(5) Van Vuuren, C. P. J.; Snyman, C. P.; Boshoff, A. J. Gold losses from cyanide solutions. Part II: The influence of the carbonaceous materials present in the shale material. Miner. Eng. 2000, 13, 1177−1181.

(6) Amankwah, R. K.; Ofori-Sarpong, G. Microwave roasting of flash flotation concentrate containing pyrite, arsenopyrite and carbonaceous matter. Miner. Eng. 2020, 151, 106312.

(7) Tan, H.; Feng, D.; Lukey, G. C.; Van Deventer, J. S. J. The behaviour of carbonaceous matter in cyanide leaching of gold. Hydrometallurgy 2005, 78, 226−235.

(8) Stenebråten, J. F.; Johnson, W. P.; Brosnahan, D. R. Characterization of Goldstrike ore carbonaceous material. Min., Metall., Explor. 1999, 16, 37−43.

(9) Ahtiainen, R.; Lundström, M.; Liipo, J. Preg-robbing verification and prevention in gold chloride-bromide leaching. Miner. Eng. 2018, 128, 153−159.

(10) Rees, K. L.; Van Deventer, J. S. J. Preg-robbing phenomena in the cyanidation of sulphide gold ores. Hydrometallurgy 2000, 58, 61−80.

(11) Ofori-Sarpong, G.; Osseo-Asare, K. Preg-robbing of gold from cyanide and non-cyanide complexes: Effect of fungi pretreatment of carbonaceous matter. Int. J. Miner. Process. 2013, 119, 27−33.

(12) Adams, M. D.; Burger, A. M. Characterization and blinding of carbonaceous preg-robbers in gold ores. Miner. Eng. 1998, 11, 919−927.

(13) Miller, J. D.; Wan, R.-Y.; Díaz, X. Preg-robbing gold ores. Dev. Miner. Process. 2005, 15, 937−972.

(14) Feng, D.; van Deventer, J. S. J. Oxidative pre-treatment in thiosulphate leaching of sulphide gold ores. Int. J. Miner. Process. 2010, 94, 28−34.

(15) Ofori-Sarpong, G.; Tien, M.; Osseo-Asare, K. Myco-hydrometallurgy: Coal model for potential reduction of preg-robbing capacity of carbonaceous gold ores using the fungus, Phanerochaete chrysosporium. Hydrometallurgy 2010, 102, 66−72.

(16) Asamoah, R. K. Specific Refractory Gold Flotation and Bio-Oxidation Products: Research Overview. Minerals 2021, 11, 93.

(17) Yang, H.-y.; Liu, Q.; Song, X.-l.; Dong, J.-k. Research status of carbonaceous matter in carbonaceous gold ores and bio-oxidation

pretreatment. *Trans. Nonferrous Met. Soc. China* **2013**, *23*, 3405−3411.

(18) Ng, W. S.; Wang, Q.; Chen, M. A review of Preg-robbing and the impact of chloride ions in the pressure oxidation of double refractory ores. *Miner. Process. Extr. Metall. Rev.* **2022**, *43*, 69−96.

(19) Wu, H.; Feng, Y.; Li, H.; Wang, H.; Ju, J. Co-recovery of manganese from pyrolusite and gold from carbonaceous gold ore using fluidized roasting coupling technology. *Chem. Eng. Process.* **2020**, *147*, 107742.

(20) Ahn, J.; Wu, J.; Ahn, J.; Lee, J. Comparative investigations on sulfidic gold ore processing: A novel biooxidation process option. *Miner. Eng.* **2019**, *140*, 105864.

(21) Amankwah, R. K.; Yen, W.-T.; Ramsay, J. A. A two-stage bacterial pretreatment process for double refractory gold ores. *Miner. Eng.* **2005**, *18*, 103−108.

(22) Guzman, I.; Thorpe, S. J.; Papangelakis, V. G. Redox potential measurement during pressure oxidation (POX) of a refractory gold ore. *Can. Metall. Q.* **2018**, *57*, 382−389.

(23) Yang, H.; Tong, L.; Yin, S. Experimental investigation on pressure preoxidation for refractory gold concentrate in Hunan with cyaniding leaching. *J. Northeast Univ., Nat. Sci.* **2007**, *28*, 1305−1308.

(24) Pak, K.-S.; Zhang, T.-A.; Kim, C.-S.; Kim, G.-H. Research on chlorination leaching of pressure-oxidized refractory gold concentrate. *Hydrometallurgy* **2020**, *194*, 105325.

(25) Xu, B.; Li, K.; Zhong, Q.; Li, Q.; Yang, Y.; Jiang, T. Study on the oxygen pressure alkaline leaching of gold with generated thiosulfate from sulfur oxidation. *Hydrometallurgy* **2018**, *177*, 178−186.

(26) Wang, H.-j.; Feng, Y.-l.; Li, H.-r.; Kang, J.-x. Simultaneous extraction of gold and zinc from refractory carbonaceous gold ore by chlorination roasting process. *Trans. Nonferrous Met. Soc. China* **2020**, *30*, 1111−1123.

(27) Wang, J.; Wang, W.; Dong, K.; Fu, Y.; Xie, F. Research on leaching of carbonaceous gold ore with copper-ammonia-thiosulfate solutions. *Miner. Eng.* **2019**, *137*, 232−240.

(28) Faraz, S.; Hossna, D.; Rezgar, B.; Piroz, Z. Improved recovery of a low-grade refractory gold ore using flotation-preoxidation-cyanidation methods. *Int. J. Min. Sci. Technol.* **2014**, *24*, 537−542.

(29) Jin, J.; Han, Y.; Li, H.; Huai, Y.; Peng, Y.; Gu, X.; Yang, W. Mineral phase and structure changes during roasting of fine-grained carbonaceous gold ores and their effects on gold leaching efficiency. *Chin. J. Chem. Eng.* **2019**, *27*, 1184−1190.

(30) Cao, Y.; Sun, Y.; Gao, P.; Han, Y.; Li, Y. Mechanism for suspension magnetization roasting of iron ore using straw-type biomass reductant. *Int. J. Min. Sci. Technol.* **2021**, *31*, 1075−1083.

(31) Qin, H.; Guo, X.; Tian, Q.; Yu, D.; Zhang, L. Recovery of gold from sulfide refractory gold ore: Oxidation roasting pretreatment and gold extraction. *Miner. Eng.* **2021**, *164*, 106822.

(32) Putz, F.; Waag, A.; Balzer, C.; Braxmeier, S.; Elsaesser, M. S.; Ludescher, L.; Paris, O.; Malfait, W. J.; Reichenauer, G.; Hüsing, N. The influence of drying and calcination on surface chemistry, pore structure and mechanical properties of hierarchically organized porous silica monoliths. *Microporous Mesoporous Mater.* **2019**, *288*, 109578.

(33) Li, H.; Ji, H.; Cui, X.; Che, X.; Zhang, Q.; Zhong, J.; Jin, R.; Wang, L.; Luo, Y. Kinetics, thermodynamics, and equilibrium of As(III), Cd(II), Cu(II) and Pb(II) adsorption using porous chitosan bead-supported $MnFe_2O_4$ nanoparticles. *Int. J. Min. Sci. Technol.* **2021**, *31*, 1107−1115.

(34) Wei, Y.; Zhang, H.; Lei, J.; Song, H.; Qi, H. Controlling pore structures of Pd-doped organosilica membranes by calcination atmosphere for gas separation. *Chin. J. Chem. Eng.* **2019**, *27*, 3036−3042.

(35) Tauetsile, P. J.; Oraby, E. A.; Eksteen, J. J. Activated carbon adsorption of gold from cyanide-starved glycine solutions containing copper. Part 1: Isotherms. *Sep. Purif. Technol.* **2019**, *211*, 594−601.

(36) Luo, Y.; Che, X.; Cui, X.; Zheng, Q.; Wang, L. Selective leaching of vanadium from V-Ti magnetite concentrates by pellet calcification roasting-H_2SO_4 leaching process. *Int. J. Min. Sci. Technol.* **2021**, *31*, 507−513.

(37) Zhang, W.; Luo, J.; Huang, Y.; Zhang, C.; Du, L.; Guo, J.; Wu, J.; Zhang, X.; Zhu, J.; Zhang, G. Synthesis of a novel dispersant with topological structure by using humic acid as raw material and its application in coal water slurry preparation. *Fuel* **2020**, *262*, 116576.

(38) Li, G.; Qin, Y.; Zhou, X.; Zhang, Y.; Hu, W. Comparative analysis of the pore structure of fusain in lignite and high-volatile bituminous coal. *J. Nat. Gas Sci. Eng.* **2021**, *90*, 103955.

(39) Wang, Z.; Jiang, X.; Pan, M.; Shi, Y. Nano-scale pore structure and its multi-fractal characteristics of tight sandstone by n2 adsorption/desorption analyses: A case study of shihezi formation from the sulige gas filed, ordos basin, china. *Minerals* **2020**, *10*, 377.

(40) Niu, H.; Yang, H.; Tong, L. Structural characterization and adsorption capability of carbonaceous matters extracted from carbonaceous gold concentrate. *Minerals* **2021**, *11*, 23.

(41) Sun, M.-M.; Zhang, J.-L.; Li, K.-J.; Li, H.-T.; Wang, Z.-M.; Jiang, C.-H.; Ren, S.; Wang, L.; Zhang, H. The Interfacial Behavior Between Coke and Liquid Iron: A Comparative Study on the Influence of Coke Pore, Carbon Structure and Ash. *JOM* **2020**, *72*, 2174−2183.

(42) Liu, X.; Li, Q.; Zhang, Y.; Jiang, T.; Yang, Y.; Xu, B.; He, Y. Simultaneous Removal of S and As from a Refractory Gold Ore in a Single Stage O2-Enriched Roasting Process. *Metall. Mater. Trans. B* **2019**, *50*, 1588−1596.